Molecular dynamics simulations of cascade damage near the $Y_2Ti_2O_7$ nanocluster/ferrite interface in nanostructured ferritic alloys*

Yi-Qiang Sun(孙祎强) and Wen-Sheng Lai(赖文生)†

Laboratory of Advanced Materials, School of Materials Science and Engineering, Tsinghua University, Beijing 100084, *China*

(Received 18 March 2017; revised manuscript received 12 April 2017; published online 6 June 2017)

A comparative study of cascades in nanostructured ferritic alloys and pure Fe is performed to reveal the influence of $Y_2Ti_2O_7$ nanocluster on cascades by molecular dynamics simulations. The cascades with energies of primary knock-on atom (PKA) ranging from 0.5 keV to 4.0 keV and PKA's distances to the interface from 0 Å to 50 Å are simulated. It turns out that the $Y_2Ti_2O_7$ nanocluster can absorb the kinetic energy of cascade atoms, prevent the cascade from extending and reduce the defect production significantly when the cascades overlap with the nanocluster. When the cascade affects seriously the nanocluster, the weak sub-cascade collisions are rebounded by the nanocluster and thus leave more interstitials in the matrix. On the contrary, when the cascade contacts weakly the nanocluster, the interface can pin the arrived interstitials and this leaves more vacancies in the matrix. Moreover, the results indicate that the $Y_2Ti_2O_7$ nanocluster keeps stable upon the displacement cascade damage.

Keywords: nanostructured ferritic alloys, molecular dynamics simulation, $Y_2Ti_2O_7$, displacement cascade

PACS: 61.80.–x, 28.41.Qb, 02.70.Ns **DOI:** 10.1088/1674-1056/26/7/076106

1. Introduction

As current fission and future fusion reactors require high performance irradiation-resistant structural materials, nanostructured ferritic alloys (NFAs), or so-called oxide dispersion strengthened (ODS) steels, are the most promising candidate materials for generation-IV nuclear reactors because of their outstanding high-temperature mechanical properties and irradiation resistance.[1–3] NFA contains a very high concentration of Y–Ti–O-enriched nanoclusters,[4,5] whose structure depends on the alloy composition and processing time–temperature history.[6] The experimental results indicate that the main compositions of the nanoclusters are $Y_2Ti_2O_7$ and Y_2TiO_5.[6–9]

Plenty of experimental researches have been performed to investigate the performance of NFA under irradiation environment, and the results indicate that the nanoclusters are stable under irradiation at high temperature and provide stable sinks for vacancy/interstitial recombination, suppressing void swelling.[10–12] However the process of defect production/annealing near the ferrite/nanoclusters interface and the mechanism of irradiation resistance enhanced by the nanoclusters are still unclear.

Many molecular dynamics (MD) simulations of displacement cascade have been done in the bulk[13,14] and near grain boundaries (GBs),[15,16] and the latter shows that GBs can serve as effective sinks for irradiation-induced defects and heal them through point-defect recombination at GBs,[15–17] whereas there are less simulations about the ferrite/oxide interfaces. An MD simulation of displacement cascade has been performed near the ferrite/Y_2O_3 nanocluster interface in ODS steels, and the results revealed that the nanocluster enhanced irradiation resistance through cascade blocking and absorbing energy.[18] Nevertheless, to our knowledge, there has no simulation about the ferrite/Y–Ti–O-enriched nanocluster interface in NFAs, such as $Y_2Ti_2O_7$ or Y_2TiO_5.

In most cases, the Y–Ti–O-enriched nanoclusters are close to stoichiometric $Y_2Ti_2O_7$,[4] which were measured by small-angle neutron scattering (SANS) in one of NFAs, named J12WYT.[6] The SANS shows that J12YWT contains the $Y_2Ti_2O_7$ nanoclusters with average radius $r = 1.6$ nm, number density $N = 3.9 \times 10^{23}$ m^{-3}, and volume fraction $f = 0.69\%$,[6] and these parameters will be adopted hereafter in our MD simulations. Different orientation relationships of ferrite/$Y_2Ti_2O_7$ are observed, including edge-on-cube and cube-on-cube bulk orientation relationships.[4] In the present study, we focus on more prevalent cube-on-cube $\{100\}\langle 100\rangle_{\mathrm{Fe}}||\{100\}\langle 100\rangle_{Y_2Ti_2O_7}$ bulk orientation relationship,[9,19] and use MD method to simulate cascade damage in NFAs and pure Fe for a comparative study. The goal is to investigate the effects of the $Y_2Ti_2O_7$ nanocluster on the cascades as well as its stability during the displacement cascades.

2. Method

2.1. Interatomic potential

In this study, different potentials are used to describe interactions between different types of atoms, and all the equi-

*Project supported by the Science Challenge Project of China (Grant No. TZ2016002) and the National Natural Science Foundation of China (Grant No. 50871057).

†Corresponding author. E-mail: wslai@tsinghua.edu.cn

© 2017 Chinese Physical Society and IOP Publishing Ltd

librium potentials are splined to the screened Coulomb potential of Ziegler–Biersack–Littmark (ZBL)[20] at very short distance. For the $Y_2Ti_2O_7$ nanocluster, a short-range Buckingham potential,[21] combined with a long-range Coulomb potential, is used to describe the Y–Ti–O (including Y–Y, Y–Ti, Y–O, Ti–Ti, Ti–O, O–O) ionic interactions, with charges being equal to +3, +4, and –2 for Y, Ti and O, respectively, and the potential parameters of Y–Ti–O are cited from Ref. [22]. For cascade simulations, the O ionic polarizability is neglected here because it is hard to be splined to the ZBL potential for both core and shell in shell model,[23] and more importantly, we have checked that such neglect does not change physical properties (e.g., lattice and elastic constants, bulk modulus) of $Y_2Ti_2O_7$ crystal.

For the Fe matrix, a Finnis and Sinclair embedded-atom method (EAM) potential developed by Mendelev *et al.*[24] is used to describe Fe–Fe interactions. For the Fe/$Y_2Ti_2O_7$ nanocluster interface, because it belongs to metal/metal oxide interactions, atomic charges and interatomic interactions depend on local chemical environments. Variable charge potential functions such as charge transfer ionic potential plus embedded-atom method (CTIP+EAM)[25,26] and charge-optimized many body (COMB)[27] potentials are more accurate for the metal/metal oxide interface interaction. However, they are very complicated to be modeled in the cascade simulations. Here, we adopt the simplified interactions, i.e., a charge-neutral Buckingham potential[28] is used to describe Fe–O interactions, while for the case of Fe–Y and Fe–Ti, because their interactions are complex (neither pure ionic nor metallic interactions), here only the ZBL potentials are used to describe Fe–Y and Fe–Ti interactions for displacement cascades. Similar simplified potentials are also adopted for cascade simulations in the ferrite/Y_2O_3 nanocluster interface in ODS steels,[18] where only the ZBL potential is used to describe Fe–Y interaction. Such simplified potentials produce the stable $Y_2Ti_2O_7$ nanocluster embedded in Fe matrix, which will be described in the next section.

For the Fe–Fe and Fe–O interactions, after the potentials are splined to the ZBL potential at a short distance and ramped the energy and force smoothly to zero at long range cutoff, they can be used directly for displacement cascade simulation. For the Y–Ti–O interactions, the potentials need to be modified so that the equilibrium potentials are smoothly splined to ZBL potential at a very short distance. The mathematical form of the potentials is adopted as follows:

$$
\begin{aligned}
V(r) &= \begin{cases} V_{\mathrm{ZBL}}(r), & r \le r_1, \\ \mathrm{e}^{\sum_{n=0}^{5} s_n r^n}, & r_1 < r < r_2, \\ V_{\mathrm{Buck}}(r) f_{\mathrm{cut}}(r) + V_{\mathrm{Coul}}(r), & r > r_2, \end{cases} \\
V_{\mathrm{Buck}}(r) &= A\mathrm{e}^{-r/\rho} - Cr^{-6}, \\
f_{\mathrm{cut}}(r) &= \begin{cases} 1, & r \le R - D, \\ \dfrac{1}{2} - \dfrac{1}{2}\sin\left(\dfrac{1}{2}\dfrac{r-R}{D}\right), & |r-R| < D, \\ 0, & r \ge R + D, \end{cases}
\end{aligned} \tag{1}
$$

where r is the distance between the two atoms; s_0–s_5 are the parameters of the spline function; r_1 and r_2 are the intervals of the exponential function; R and D are the parameters of the damping function ramped to zero at $r = R + D$; $V_{\mathrm{Coul}}(r)$ is the long-range Coulomb interaction, which decays slowly with r. The parameters of Buckingham potential A, ρ, and C for $Y_2Ti_2O_7$ are cited from Ref. [22].

In the bulk $Y_2Ti_2O_7$ lattice, the summation of Coulomb interaction can be calculated by Ewald summation method.[29] However, it does not work in the $Y_2Ti_2O_7$ nanocluster because of truncation of long-range periodicity. In the present study, the Coulomb interaction is computed via the damped shifted force model described by Fennell[30]

$$
\begin{aligned}
V_{\mathrm{Coul}}(r) = q_i q_j \Bigg[& \frac{\mathrm{erfc}(\alpha r)}{r} - \frac{\mathrm{erfc}(\alpha r_{\mathrm{c}})}{r_{\mathrm{c}}} \\
& + \left(\frac{\mathrm{erfc}(\alpha r_{\mathrm{c}})}{r_{\mathrm{c}}^2} + \frac{2\alpha}{\sqrt{\pi}} \frac{\exp\left(-\alpha^2 r_{\mathrm{c}}^2\right)}{r_{\mathrm{c}}} \right) (r - r_{\mathrm{c}}) \Bigg], \\
& r < r_{\mathrm{c}},
\end{aligned} \tag{2}
$$

where α is the damping parameter and erfc( ) is the complementary error-function. This potential provides consistent forces and energies and decays smoothly to zero at the cutoff radius r_{c}. The $\alpha = 0.2$ Å^{-1} and $r_{\mathrm{c}} = 12$ Å are chosen in this work.

The r_1, r_2, and s_0–s_5 are fitted by smoothly connecting the exponential function and its derivative to ZBL potential at r_1 and the equilibrium potential at r_2, respectively. The determined parameters of the spline function for Y–Ti–O potentials are given in Table 1 and the values of r_1, r_2 and damping function parameters R and D are given in Table 2.

Table 1. Parameters of the spline function for Y–Ti–O potentials.

Type	s_0	s_1/Å^{-1}	s_2/Å^{-2}	s_3/Å^{-3}	s_4/Å^{-4}	s_5/Å^{-5}
Y–Y	41.509	–165.189	322.171	–318.565	154.532	–29.201
Y–Ti	84.569	–456.670	1078.947	–1273.297	740.824	–169.426
Y–O	123.843	–906.024	2761.828	–4116.037	2972.585	–834.483
Ti–Ti	21.022	–98.684	301.686	–482.519	378.625	–115.009
Ti–O	177.637	–1396.876	4521.263	–7233.306	5696.032	–1769.508
O–O	5.518	14.451	–58.998	77.566	–43.338	8.779

Table 2. Values of r_1, r_2 and damping function parameters R and D. All units are in Å.

Type	Fe–Y	Fe–Ti	Y–Y	Y–Ti	Y–O	Ti–Ti	Ti–O	O–O
r_1	–	–	0.8	0.7	0.5	0.6	0.5	0.5
r_2	–	–	1.4	1.1	1.0	0.9	0.8	1.5
R	3.5	3.5	9.1	9.1	9.1	9.1	9.1	9.1
D	0.5	0.5	0.1	0.1	0.1	0.1	0.1	0.1

2.2. NFAs' structural model

$Y_2Ti_2O_7$ has a pyrochlore structure ($Fd\bar{3}m$, O_h^7) and atoms occupy the following Wyckoff sites: Ti at 16c (0, 0, 0), Y at 16d (1/2, 1/2, 1/2), O at 48f (δ, 1/8, 1/8), and O′ at 8b (3/8, 3/8, 3/8). O and O′ atoms occupy two non-equivalent chemical environments: O is located in a tetrahedron composed of two Y atoms and two Ti atoms; O′ is situated in a tetrahedron composed of four Y atoms. Lattice constant a = 10.0988 Å and O displacement $\delta = 0.3277$ which were measured experimentally[31] are used to construct the $Y_2Ti_2O_7$ unit cell. Geometry optimization through the above potentials with constant pressure gives a = 10.0622 Å and $\delta = 0.3223$, in consistent with the experimental values. Figure 1 shows the pyrochlore lattice of $Y_2Ti_2O_7$ after structural relaxation.

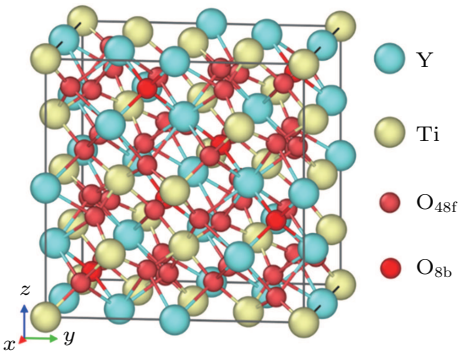


Fig. 1. (color online) Crystal structure of $Y_2Ti_2O_7$ after structural relaxation. Two non-equivalent O atoms are indicated by O_{48f} and O_{8b}.

In order to accurately simulate cascade damage to NFAs, we construct a model of NFAs structure by using the parameters deduced from experimental observation[6] as mentioned above. The model consists of a sphere $Y_2Ti_2O_7$ nanocluster ($r = 16$ Å) embedded with cube-on-cube $\{100\}\langle 100\rangle_{Fe}||\{100\}\langle 100\rangle_{Y_2Ti_2O_7}$ orientation in the center of a bcc Fe matrix (137 Å × 137 Å × 137 Å) as shown in Fig. 2. Such an orientation relationship has been adopted to establish the Fe/$Y_2Ti_2O_7$ interface in the first-principles calculation.[32] The "structure matching" method,[33] which has been used in building the smallest NFAs model for *ab initio* study, is adopted to construct the model in the following ways. Firstly, a sphere $Y_2Ti_2O_7$ nanocluster is created by choosing atoms within a range of a radius of 16 Å from an $Y_2Ti_2O_7$ matrix, and performing an energy minimization in the vacuum. Secondly, it is embedded in the Fe matrix by removing the Fe atoms whose positions are overlapped with the nanocluster. Moreover, in order to avoid Fe atoms being too close to the nanocluster surface, those Fe atoms with distances less than 1.5 Å to the nanocluster surface are also removed. Finally the model is fully relaxed to obtain a stable structure of NFAs for cascade simulations.

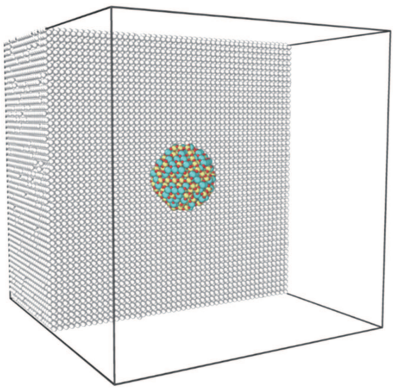


Fig. 2. (color online) Stable structure of the NFA model after relaxation in this work. For a clear view, only half of Fe atoms are shown.

2.3. MD simulation of cascade damage in the NFA

All the simulations are performed by the classical MD code LAMMPS,[34] and the simulation data are analyzed and visualized by OVITO.[35] Periodic boundary condition (PBC) is applied to three directions of the NFA model so that the number density and volume fraction of $Y_2Ti_2O_7$ nanoclusters are the same as those of J12YWT. The model is firstly relaxed at $T = 300$ K for 30 ps in NPT ensemble to remove the remanent stress, and then relaxed in NVT ensemble for phone equilibrium in the next 20 ps before starting the displacement cascade with constant NVE ensemble. The time step varies from 0.1 fs to 1 fs, and the total simulation time lasts 20 ps for displacement cascade simulation. To study the effect of primary knock-on atom (PKA) positions on defect productions, six PKAs with the same energy of 2.0 keV at different positions with the values of distance, d, ranging from 0 Å to 50 Å with the same interval of 10 Å to the interface are chosen, and a high index $\langle 135\rangle$ incident direction is used to minimize the channeling effect as shown in Fig. 3. To investigate the effect of PKA energy on defect production, the cascade simulations for three PKAs with $d = 10$ Å, 20 Å, 30 Å and different values of PKA energy, E_p, of 0.5 keV, 1.0 keV, 2.0 keV, 3.0 keV, and 4.0 keV are conducted. The ten independent simulations are performed for each type of simulations in order to reduce the statistical error.

The defect analysis is done by using the Wigner–Seitz (WS) cell method, which can identify point defects (vacancies and interstitials) and count them in a crystal. The reference lattice is obtained by quenching the model at 0 K before the start of cascade simulation. As the cascade simulation causes a reconstruction of the interface, to avoid counting rearrangements of Fe in the interface as defects, we only count defects

in the matrix. The width of the interface is obtained by using common neighbor analysis (CNA),[36] which is an algorithm to characterize local structural environment. Those Fe atoms with CNA index different from those of the matrix bcc Fe atoms are identified as interfacial atoms, and we find that a width of 4 Å is suitable as shown in Fig. 3.

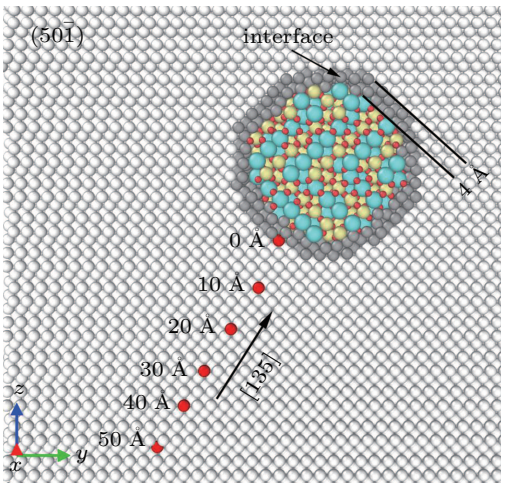


Fig. 3. (color online) Schematic diagram of the Fe/nanocluster interface and PKA positions. The cutting plane is (50$\bar{1}$), the width of interface is 4 Å, and six PKAs with distances ranging from 0 Å to 50 Å to the interface along [135] direction are shown for cascade simulations.

3. Results and discussion

3.1. Effect of the nanocluster on the cascade

3.1.1. Effect of PKA distance

Figure 4(a) shows variation of the number of surviving defects (interstitials and vacancies) in the matrix of the NFA with PKA distance d at the fixed $E_p = 2.0$ keV, together with the average number of Frenkel pairs in pure Fe for comparison. It can be seen that the number of defects in the NFA shows a significant reduction and is less than that in pure Fe when $d < 30$ Å, suggesting that the nanocluster can reduce the defect production significantly when the PKA is close to it. It can also be seen that the number of interstitials is slightly smaller than that of vacancies when $d = 30$ Å.

To better understand the reason for the above results, we plot the process of the defects evolution with the time in Fig. 4(b) at the fixed $E_p = 2.0$ keV and $d = 10$ Å. It shows that the number of interstitials and the number of vacancies in the NFA increase slowly compared with that of Frenkel pairs in pure Fe at collision stage, reach a maximum value of 46.4 for interstitials and 36.1 for vacancies in the NFA at defect spike stage, much less than the value of 127.3 for Frenkel pairs in pure Fe, and then decrease with increasing the time at the stage of recombination of the interstitials and vacancies, leaving the remnant number of interstitials and vacancies less than that of Frenkel pairs in pure Fe.

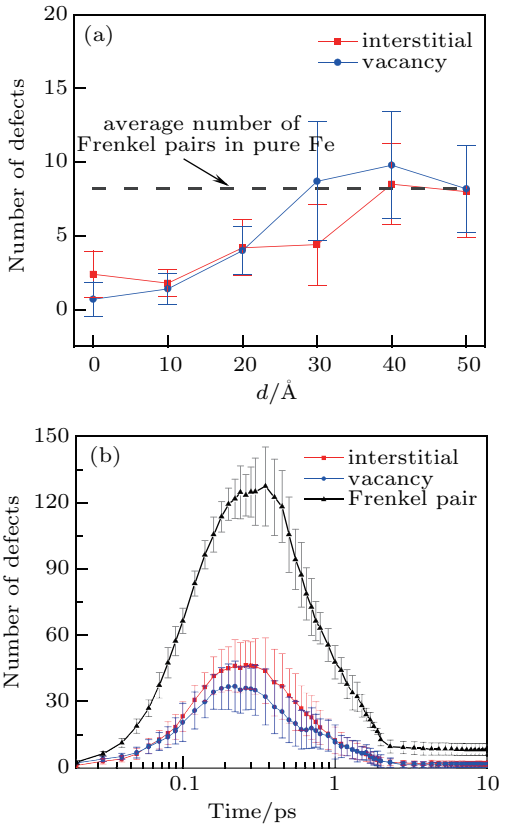


Fig. 4. (color online) (a) Variation of the number of surviving defects in the matrix of the NFA with d after 20 ps. The number of defects in pure Fe with the same PKA orientation and energy is indicated by the horizontal dash line. (b) Evolution of the number of defects with the time during the first 10 ps of cascade in the NFA with $d = 10$ Å and in pure Fe (the black line). $E_p = 2.0$ keV for both panels (a) and (b).

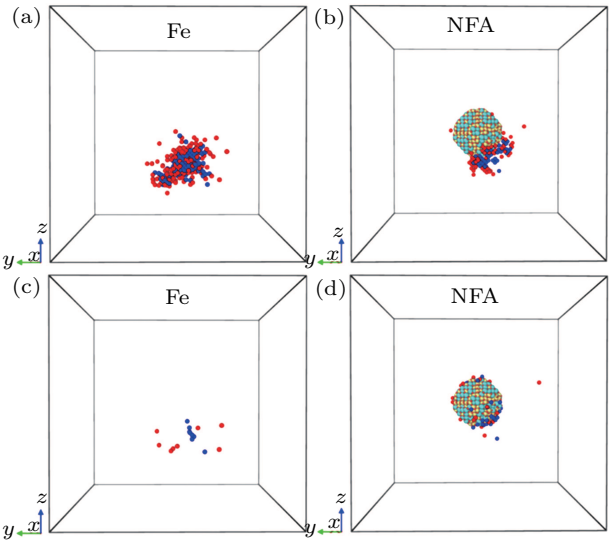


Fig. 5. (color online) Snapshots of defect configurations at different times of cascade simulations for pure Fe and the NFA with $E_p = 2.0$ keV, ((a), (b)) at defect spike stage, and ((c), (d)) at 20 ps. Red spheres are Fe interstitials, blue spheres are Fe vacancies, and those Fe atoms on lattice sites are not shown. Those defects in the interface region identified via WS cell method are shown for an intuitive view of interface structure change upon cascade damage, yet they are not counted in defect statistics of the matrix. The figure chooses the data in one of 10 simulations, which are closest to average value.

Figure 5 shows the snapshots of defect configurations at different times for the cascade simulations in Fig. 4(b). It can

be observed that partial cascade region is overlapped with the nanocluster as shown in Fig. 5(b). It can also be seen from Figs. 5(c) and 5(d) that the number of defects in the matrix of the NFA (2 interstitials +1 vacancy) is much less than that (8 interstitials +8 vacancies) in pure Fe. To demonstrate how cascades affect the interface structure, those defects in the interface region identified via WS cell method are also shown in Figs. 5(b) and 5(d), yet they have not been counted in defect statistics of the matrix. Moreover, in our cascade simulations with $E_p \leq 4.0$ keV, we observe that rarely Fe atoms can penetrate into the nanocluster and almost all Fe atoms stay in Fe matrix or the interface region next to $Y_2Ti_2O_7$ nanocluster.

In order to investigate the energy transfer, we further analyze the temperature changes of $Y_2Ti_2O_7$ nanocluster and Fe matrix during the displacement cascade. The results are shown in Fig. 6, together with the distribution of mean kinetic energies along x and y axis averaged along the z direction at 0.2 ps. It can be seen that the temperature of $Y_2Ti_2O_7$ nanocluster rapidly rises at the early stage of cascade and then slowly drops with the simulation time increasing. The average temperature of Fe matrix remains almost unchanged. The underlying physics process is as follows: the nanocluster first rapidly absorbs a great quantity of the kinetic energies of cascade atoms at cascade stage as evidenced by rapid temperature rise and the inset of Fig. 6, and then slowly releases its kinetic energy to the Fe matrix through phonon conduction.

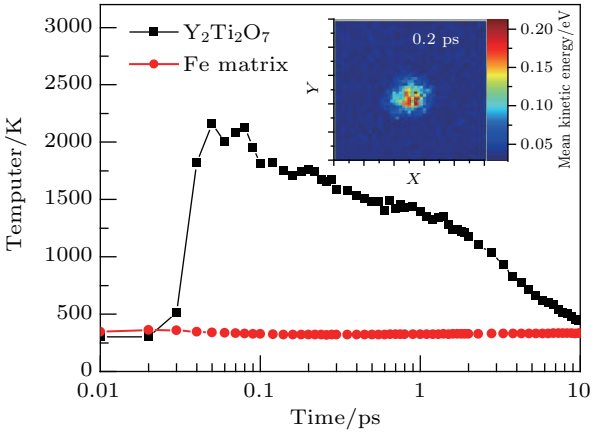


Fig. 6. (color online) Variations of the average temperature with time in $Y_2Ti_2O_7$ nanocluster and Fe matrix. $E_p = 2.0$ keV and $d = 10$ Å. Inset shows the distribution of mean kinetic energies along x and y axis averaged along the z direction at 0.2 ps.

The above results clearly show that the nanocluster can absorb the kinetic energy of the cascade atoms, prevent cascades from extending and reduce the defect production in the matrix of the NFA. In other words, the Fe/$Y_2Ti_2O_7$ interface can pin the cascade atoms created in the matrix near the interface, so the dispersion distributed oxide nanoclusters can act as the sinks for interstitials and vacancies, significantly reducing the number of interstitials and vacancies in the matrix and thus enhancing neutron irradiation-resistance property of the NFAs. Moreover, as the Fe/oxide nanocluster interfaces can pin interstitials, such a behavior prevents the interstitials from escaping to the surfaces or forming dislocation loops in the matrix, and eventually reduces radiation-induced swelling property of the NFAs.

3.1.2. Effect of PKA energy

To further investigate the effect of PKA energy, we perform the MD simulations with different values of E_p at 3 different values of d (namely, 10 Å, 20 Å, and 30 Å), and the results are shown in Fig. 7 together with those in pure Fe for comparison. In these simulations, we observe that almost all Fe atoms do not penetrate into the nanocluster and no Y, Ti, and O atoms are rebounded into Fe matrix either. It can be seen from Fig. 7 that the number of defects in pure Fe increases almost linearly with increasing E_p from 0.5 keV to 4.0 keV. From Fig. 7(a), it can be seen that in the NFA the number of interstitials keeps almost unchanged with the same quantity as that of vacancies when $E_p < 3.0$ keV and then increases slightly faster than that of vacancies with increasing E_p (≥ 3.0 keV) and that the number of defects in the NFA is less than that in pure Fe. From Fig. 7(b), it can be seen that in the NFA both the number of interstitials and the number of vacancies keep nearly unchanged with the increase of E_p, and are almost slightly less than that in pure Fe. From Fig. 7(c), it can be seen that in the NFA with increasing E_p the number of interstitials increases linearly with a slope slightly smaller than pure Fe, and that the number of vacancies increases with the same step as that in pure Fe when $E_p \leq 2.0$ keV, and becomes almost the same (overlapped) when $E_p \geq 3.0$ keV.

Generally, the increase of E_p will produce more interstitials and vacancies as clearly evidenced in pure Fe. When the PKA position is close to the Fe/nanocluster interface at $d = 10$ Å (see Fig. 7(a)), the cascades overlap more seriously with the nanocluster with increasing E_p, resulting in severe collisions between the cascade atoms and the nanocluster. This will cause some small rebounded sub-cascade collisions, which produce a little more interstitials back to the matrix as compared with vacancies in Fe matrix.

When the PKA position is at $d = 20$ Å (see Fig. 7(b)), the cascades produce almost the same interstitials and vacancies in the matrix, independent of E_p. When the PKAs are located at suitable positions, the increase of E_p will create more vacancies and atomic flux towards the nanocluster. Moreover the contacted area between the atomic flux and the nanocluster increases with increasing E_p. The collisions of atomic flux with the nanocluster will rebound Fe atoms back to the matrix, resulting in almost unchanged defect numbers due to the recombination of interstitials with vacancies.

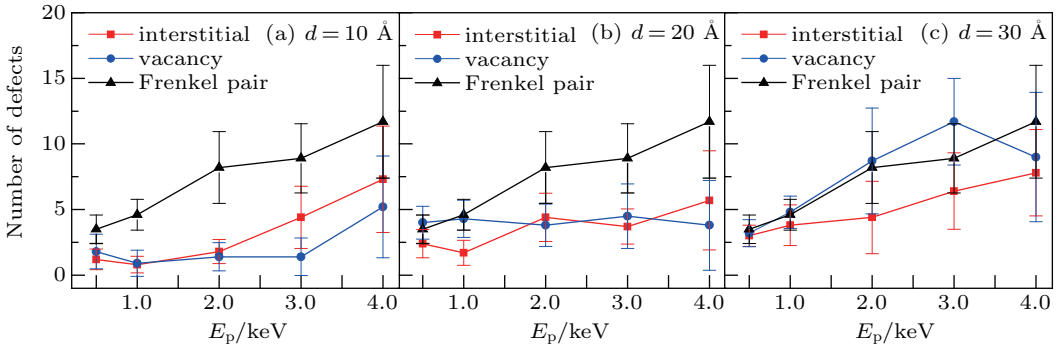


Fig. 7. (color online) Variations of the number of surviving defects in the matrix of the NFA with E_p for the different PKA positions at (a) $d = 10$ Å, (b) 20 Å, and (c) 30 Å after 20 ps. The black line obtained in pure Fe is also shown for comparison.

When the PKA position is at d = 30 Å, a little far away from the interface (see Fig. 7(c)), the number of vacancies and the number of interstitials are both nearly the same as that of Frenkel pairs at E_p = 0.5 keV, because of no overlap between cascades and the nanocluster. With the increase of E_p, the number of interstitials increases slightly slower than that of vacancies, which is almost the same as the scenario of Frenkel pairs in pure Fe when $E_p < 2.0$ keV. This is because some of interstitials can reach and be pinned by the interface.

From Fig. 7, it can be found that the number of interstitials is slightly more than that of vacancies when d is small and E_p is high, and vice versa when the d is big and the E_p is low. The small d and high E_p cause serious overlap (or collision) between cascade (or Fe atoms) and the nanocluster, resulting in more weak rebound of Fe atoms and thus more surviving interstitials. Whereas the large d and low E_p cause weak collision between Fe atoms and the nanocluster, leaving more vacancies in the matrix due to the pinning effect of the Fe interstitials by the interface. To better understand the underlying mechanisms, we choose two typical cases from Fig. 7, i.e., $E_p = 3.0$ keV and $d = 10$ Å in Fig. 7(a), and $E_p = 3.0$ keV and $d = 30$ Å in Fig. 7(c), and then draw the displacement vectors of Fe atoms after PKA run at 20 ps in Fig. 8. It can be seen from Fig. 8(a) that the extension of the cascade toward original direction is hindered by the nanocluster and turns into some weak sub-cascade collisions in other directions, leaving the more interstitials in the matrix. Figure 8(b) shows that the cascade just has a small overlap with the nanocluster and some cascade atoms are absorbed and pinned by the interface, leaving more vacancies in the matrix. The role of the Fe/nanocluster interface is similar to that of the GBs,[16] which can absorb or emit the interstitials.

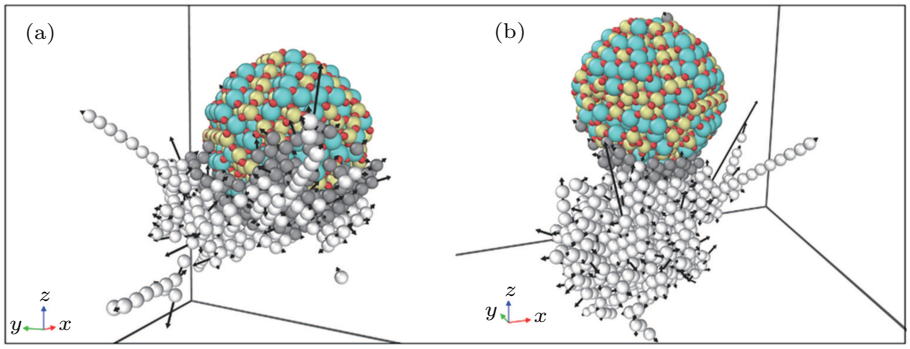


Fig. 8. (color online) Displacement vectors of Fe atoms in the NFA after PKA run with $E_p = 3.0$ keV at 20 ps for (a) $d = 10$ Å and (b) $d = 30$ Å. Displacement length of Fe less than 2 Å is not shown. Direction of vector represents the displacement direction and the length of vector represents the displacement size. The grey and white spheres denote Fe atoms in the interface and the matrix, respectively.

3.2. Stability of the nanocluster

The stability of the nanocluster under radiation is also very important as it will influence its role of reducing the number of surviving defects in the NFAs. In order to maximize the test result for the stability of the nanocluster, we choose a PKA with high energy ($E_p = 4.0$ keV) and short distance ($d = 10$ Å) to the interface. The stability of the nanocluster can be analyzed by the radial distribution function (RDF), which is plotted for Y, Ti, and O atoms within this nanocluster in Fig. 9. It can be seen that the nanocluster turns disordered at defect spike stage (peak) and then almost recovers its initial state at the end of the cascade.

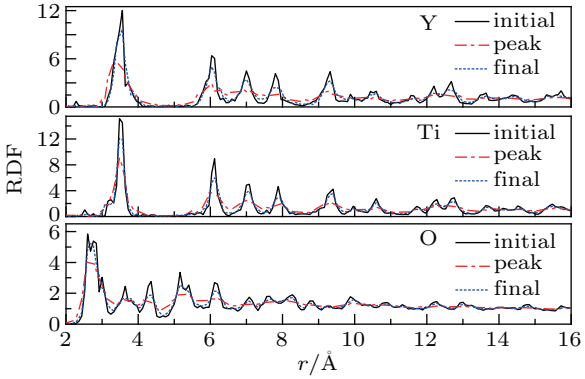


Fig. 9. (color online) Radial pair distribution functions (RDFs) for Y, Ti, and O atoms in the nanocluster with $E_p = 4.0$ keV and $d = 10$ Å. The nanocluster is the most disordered at peak (defect spike stage).

4. Conclusions

In this paper, displacement cascades near the Fe/$Y_2Ti_2O_7$ nanocluster interface in the NFA are simulated by MD method to investigate the role of the $Y_2Ti_2O_7$ nanoclusters in defect production as well as its stability under irradiation. The results indicate that the nanoclusters can absorb the kinetic energy of the cascade atoms, prevent the cascades from extending and reduce the defect production significantly when the cascade has an overlap with the nanocluster, and thus enhance the irradiation resistance of NFAs. The number of surviving defects in the matrix of NFAs, which is related to the PKA energy and its distance to the interface, decreases nearly with reducing the PKA's distance to the interface and increases with increasing the PKA energy. When the cascade affects the nanocluster seriously, weak sub-cascade collisions are rebounded by the nanocluster and thus leave more interstitials in the matrix. On the contrary, when the cascade contacts the nanocluster weakly, the interface can pin the interstitials reaching interface, which leaves more vacancies in the matrix. The nanocluster turns disordered at defect spike stage and then almost recovers its initial state at the end of the cascade.

References

[1] Lindau R, Moslang A, Rieth M, Klimiankou M, Materna-Morris E, Alamo A, Tavassoli A a F, Cayron C, Lancha A M, Fernandez P, Baluc N, Schaublin R, Diegele E, Filacchioni G, Rensman J W, Van Der Schaaf B, Lucon E and Dietz W 2005 *Fusion Eng. Des.* **75** 989

[2] Odette G R, Alinger M J and Wirth B D 2008 *Annu. Rev. Mater. Res.* **38** 471

[3] Murty K L and Charit I 2008 *J. Nucl. Mater.* **383** 189

[4] Odette G R 2014 *Jom* **66** 2427

[5] Hirata A, Fujita T, Wen Y R, Schneibel J H, Liu C T and Chen M W 2011 *Nat. Mater.* **10** 922

[6] Alinger M J, Odette G R and Hoelzer D T 2009 *Acta Mater.* **57** 392

[7] Wu Y, Haney E M, Cunningham N J and Odette G R 2012 *Acta Mater.* **60** 3456

[8] Bhattacharyya D, Dickerson P, Odette G R, Maloy S A, Misra A and Nastasi M A 2012 *Philos. Mag.* **92** 2089

[9] Dawson K and Tatlock G J 2014 *J. Nucl. Mater.* **444** 252

[10] Miller M K, Hoelzer D T, Kenik E A and Russell K F 2005 *Intermetallics* **13** 387

[11] Alinger M J, Odette G R and Hoelzer D T 2004 *J. Nucl. Mater.* **329** 382

[12] Odette G R and Hoelzer D T 2010 *Jom* **62** 84

[13] Yu G, Ma Y, Cai J and Lu D G 2012 *Chin. Phys. B* **21** 036101

[14] Li W N, Xue J M, Wang J X and Duan H L 2014 *Chin. Phys. B* **23** 036101

[15] Chen D, Wang J, Chen T Y and Shao L 2013 *Sci. Rep.* **3** 1450

[16] Bai X M, Voter A F, Hoagland R G, Nastasi M and Uberuaga B P 2010 *Science* **327** 1631

[17] Chen Y, Yu K Y, Liu Y, Shao S, Wang H, Kirk M A, Wang J and Zhang X 2015 *Nat. Commun.* **6** 7036

[18] Lazauskas T, Kenny S D, Smith R, Nagra G, Dholakia M and Valsakumar M C 2013 *J. Nucl. Mater.* **437** 317

[19] Ribis J and De Carlan Y 2012 *Acta Mater.* **60** 238

[20] Ziegler J F, Biersack J P and Littmark U 1985 *The Stopping and Range of Ions in Matter* (New York: Pergamon Press) pp. 14–65

[21] Lewis G V and Catlow C R A 1985 *J. Phys. C: Solid State Phys.* **18** 1149

[22] Minervini L, Grimes R W and Sickafus K E 2000 *J. Am. Ceram. Soc.* **83** 1873

[23] Dick B G and Overhauser A W 1958 *Phys. Rev.* **112** 90

[24] Mendelev M I, Han S, Srolovitz D J, Ackland G J, Sun D Y and Asta M 2003 *Philos. Mag.* **83** 3977

[25] Zhou X W, Wadley H N G, Filhol J S and Neurock M N 2004 *Phys. Rev. B* **69** 035402

[26] Nalepka K 2012 *Eur. Phys. J. B* **85** 45

[27] Liang T, Shan T R, Cheng Y T, Devine B D, Noordhoek M, Li Y Z, Lu Z Z, Phillpot S R and Sinnott S B 2013 *Mat. Sci. Eng. R* **74** 255

[28] Hammond K D, Voigt H J L, Marus L A, Juslin N and Wirth B D 2013 *J. Phys.: Condens. Matter* **25** 055402

[29] Ewald P P 1921 *Ann. Phys.* **369** 253

[30] Fennell C J and Gezelter J D 2006 *J. Chem. Phys.* **124** 234104

[31] Matteucci F, Cruciani G, Dondi M, Baldi G and Barzanti A 2007 *Acta Mater.* **55** 2229

[32] Yang L T, Jiang Y, Wu Y, Odette G R, Zhou Z J and Lu Z 2016 *Acta Mater.* **103** 474

[33] Barnard L, Odette G R, Szlufarska I and Morgan D 2012 *Acta Mater.* **60** 935

[34] Plimpton S 1995 *J. Comput. Phys.* **117** 1

[35] Stukowski A 2010 *Model. Simul. Mater. Sci. Eng.* **18** 015012

[36] Honeycutt J D and Andersen H C 1987 *J. Phys. Chem.* **91** 4950